Electronic Supplementary Information

N-doped carbon nanotube as an efficient electrocatalyst for O_2 conversion to H_2O_2 in neutral electrolyte

Sijia Ren,[a,b] Wenxin Cui,[a] Lixin Li,[a] Zhiguo Yi*[a]

[a] State Key Laboratory of High Performance Ceramics and Superfine Microstructure, Shanghai Institute of Ceramics, Chinese Academy of Sciences, Shanghai, China. Email: zhiguo@mail.sic.ac.cn

[b] Center of Materials Science and Optoelectronics Engineering, University of Chinese Academy of Sciences, Beijing, China

Experimental Section

Materials: Carbon nanotubes was bought from graphenechina. Urea, dibasic Sodium Phosphate (Na_2HPO_4), potassium dihydrogen phosphate (KH_2PO_4), potassium hydroxide (KOH), Isopropyl alcohol (IPA) were bought from Aladdin Ltd. Carbon paper were bought from Beijing Chemical Corporation. Nafion (5 wt%) were purchased from Sigma-Aldrich Chemical Reagent Co., Ltd. The water used throughout all experiments was purified through a Millipore system. The purity of the above drugs is analytically pure and has not been further purified.

Preparation of N-CNT: First, 20 mg carbon nanotube were ultrasonicated in 40 mL deionized water for 30 min. Then, 1 g urea were added under vigorous stirring. After being magnetically stirred for 30 min in air at room temperature, the mixture solution was transferred to a Teflon-lined stainless-steel autoclave and maintained at 180 °C for 8 h. After the autoclave naturally cooled down to room temperature, the sample was collected by centrifugation and thoroughly washed with deionized water several times, then dried in air at 60 °C.

Characterization: X-ray diffraction (XRD) patterns were collected from a Shimadzu XRD-6100 diffractometer with Cu Kα radiation (40 kV, 30 mA) of wavelength 0.154 nm (Japan). Scanning Electron Microscopy (SEM) images were obtained using a Quanta FEG 250 field-emission SEM with an accelerating voltage of 20 kV. Transmission Electron Microscopy (TEM) images were obtained from a Zeiss Libra 200FE transmission electron microscope operated at 200 kV. X-Ray Photoelectron Spectroscopy (XPS) measurements were performed on an ESCALABMK II X-ray photoelectron spectrometer using Mg as the exciting source. Raman spectra were performed using a Horiba-Xplora Plus confocal microscope with 20 × (0.25 NA) objective. A 532 nm laser (1-20 mW) was focused on the electrode, and the Raman scattered photons were dispersed by 1,800 g cm^{-1} grating and collected by a spectrometer.

Electrochemical measurements: The electrochemical measurements were performed

using an electrochemical workstation (CHI760E, CH Instruments). For the rotating ring disk electrode (RRDE) measurements, a three-electrode system was built with an RRDE (glassy carbon (GC) disk+Pt ring), a Hg/HgO reference electrode, and a graphite rod counter electrode. For the accurate and reproducible measurement of H_2O_2 selectivity, it is very important to clean the RRDE thoroughly prior to each experiment. The RRDE was polished with 1 um alumina aqueous suspension for 5 min and 0.05 um alumina aqueous suspension for 5 min and ultra-sonicated in deionized water for 30 s. The catalyst ink was prepared by mixing the catalyst with water, 2-propanol, and Nafion (5 wt%) (v/v/v = 4/1/0.02) to form a 4 mg mL^{-1} suspension. After sonication for 60 min, 5 ul of the catalyst ink was drop-dried onto a glassy carbon disc (disk area: 0.2462 cm^2 ； ring area：0.1866 cm^2). Cyclic voltammetry (CV) was performed between 0.2 and 1.20 V (vs. RHE) in N_2-saturated 0.1 M PBS at a scan rate of 100 mV s^{-1} for 40 cycles, in which a steady CV response was obtained. Pt ring was then electrochemically cleaned in the same potential range at a scan rate of 500 mV s^{-1} for 10 cycles. O_2 gas was purged into the electrolyte for 5 min (caution: if the time interval between the Pt ring cleaning and ORR measurement is long, the H_2O_2 selectivity can be underestimated due to the surface passivation of the Pt ring). The H_2O_2 production activity was assessed by linear sweep voltammetry (LSV) from 0.2 to 1.2 V (vs. RHE) in O_2-saturated 0.1 M PBS at a scan rate of 20 mV s^{-1} and a rotation speed of 1600 r.p.m. During the LSV, the Pt ring potential was held at 1.2 V (vs. RHE). Polarization curves in nitrogen-saturated electrolytes were also recorded as a reference.

The H_2O_2 selectivity was calculated using the following relation:

$$H_2O_2\ (\%) = 200 \times I_r / N / (I_d + I_r / N) \qquad (1)$$

where I_r is the ring current, I_d is the disk current and N is the collection efficiency (0.35 after calibration). The collection efficiency (N) was determined using the $[Fe(CN)_6]^{3-/4-}$ redox system. The catalyst-deposited RRDE was soaked in N_2-saturated 0.1 M KNO_3 + 10 mM $K_3[Fe(CN)_6]$, and chronoamperometry was performed at -0.3 V (vs. Hg/HgO) while the ring potential was fixed at 0.5 V (vs. Hg/HgO) for 50 s. The background response was also obtained similarly, but the applied disk potential was 0.5 V (vs. Hg/HgO). The collection efficiency could be calculated as follows:

$$N = (|i_r - i_{r,bg}|) / i_d \quad (2)$$

where $i_{r, bg}$ stands for the background ring current. The result yields that the collection efficiency is 35%. The kinetic current (I_k) was extracted by correcting the mass transport losses, according to the equation:

$$1/I_m = 1/I_l + 1/I_k \quad (3)$$

where I_m indicates the measured total current and I_l is the diffusion-limited current. Usually, it is difficult to determine the value of the limiting current, usually determined from the highest steady current measured in the entire potential range, in most of the carbonaceous catalysts. Thus, we calculated the limiting current from the Levich equations with the total electron transfer number (n) obtained from our RRDE system. The Levich equation is:

$$I_l = 0.62nFAD_o^{2/3}\omega^{1/2}\upsilon^{-1/6}C_o \quad (4)$$

F, A, D_o, ω, υ and C_o indicate the Faraday constant (96,485 C mol^{-1}), geometric area of the disk electrode (0.2462 cm^2), diffusion coefficient of O_2 in the electrolyte at 298 K (1.85×10^{-5} cm^2 s^{-1}), electrode rotation speed (rad s^{-1}), kinematic viscosity of O_2 (0.89×10^{-2} cm^2 s^{-1}) and O_2 concentration (1.21×10^{-6} mol cm^{-3}). The mass activity was calculated at 0.65 V and at 0.75 V with an electrode rotation speed of 1,600 r.p.m.

Electrogeneration of H_2O_2: The electrogeneration of H_2O_2 were conducted in flow cell setup in a two-compartment cell with nafion 117 membrane as separator. Cathode was prepared by depositing catalyst ink (0.05 mg cm^{-2}) on a carbon paper (1 by 1 cm) and platinum wire is used as anode.

To quantify the H_2O_2 produced, the samples was collected at certain time and mixed with same volume of titanium oxysulfate solution (6 g L^{-1}). The H_2O_2 yield was measured by using the indicator of titanium oxysulfate. The generated complex compound solution was detected with UV-vis spectrophotometer (UV-8000, METASH.) at the maximum absorption wavelength λ= 406 nm. The FE for H_2O_2 generation in H-cell was calculated as follows:

$$FE\% = \frac{mole\ of\ generation\ H_2O_2 \times 2 \times 96485}{total\ consumed\ charge\ (C)} \quad (5)$$

Computational Details: The spin-polarized density functional theory (DFT)

calculations were performed with Vienna ab initio simulation package (VASP).[1] The interactions between the valence electrons and the ion cores were described by the projected augment wave (PAW) pseudopotential[2] and the exchange-correlation effects by the Perdew, Burke, and Ernzerhof (PBE) functional.[3] The van der Waals (vdW) interaction was included by using the DFT+D3 method.[4] The plane-wave basis was used with a kinetic energy cutoff of 450 eV. The convergence criteria for the total energy and the Hellmann-Feynman force are 10^{-5} eV and 0.02 eVÅ^{-1}, respectively. To consider the edge effect, two typical graphene nanoribbons have been adopted: the armchair and zigzag graphene nanoribbons, with the ribbon widths of ~ 14 Å, denoted as AGNR and ZGNR, respectively. In addition, the pristine graphene sheet with the (6×6) supercell (denoted as Gr) is also investigated. For all the models, the vacuum layers were set to be larger than 15 Å, to avoid the interaction between slabs. The Brillouin zone was sampled using the Monkhorst-Pack grids[5] of (1×2×1), (2×1×1), and (2×2×1), respectively, for AGNR, ZGNR, and Gr.

The binding strength for the OOH* (ΔG_{HOO*}) is considered to be the best descriptor to evaluate the activity of 2e$^-$ ORR.[6-9] For the calculation of ΔG_{HOO*}, we have adopted the computational hydrogen electrode (CHE) model,[10] using the equation: $\Delta G = \Delta E + \Delta E_{ZPE} - T\Delta S$, where E, E_{ZPE}, and S denotes the total electronic energy, zero-point energy, and entropy of the relevant systems, respectively, and T is taken as 298.15 K. E_{ZPE} and S of the adsorbed intermediates were obtained from DFT calculations, while those of the free molecules (H_2 and H_2O) taken from the NIST databases.[11] It is noted that the solvation effect may bring a small stabilization on the adsorbed OOH, while the reported activity trend should keep unchanged without the solvation correction. In fact, although in the previous works on the 2e$^-$ ORR[6-9] DFT calculations did not consider the solvation effect, the good agreement between the experimental and theoretical results were observed. Therefore, as previous works,[6-9] herein we did not consider the solvation effect in determining the value of ΔG_{HOO*}, which in turn allows us to make a direct comparison with the previous results.[6-9]

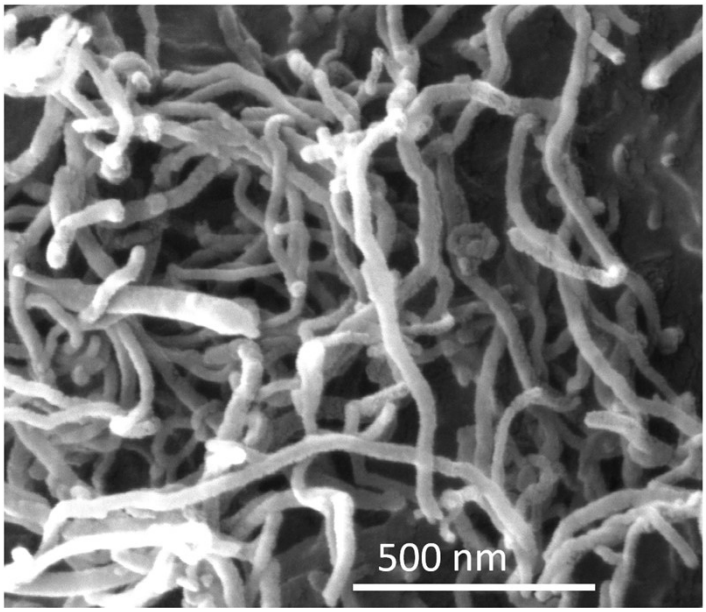

Fig. S1. SEM image of N-CNT.

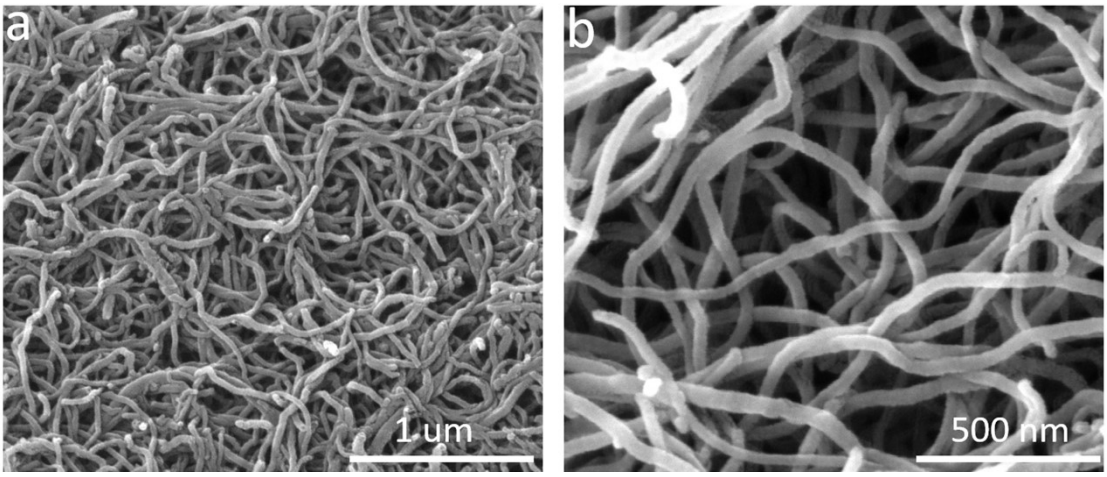

Fig. S2. SEM images of CNT.

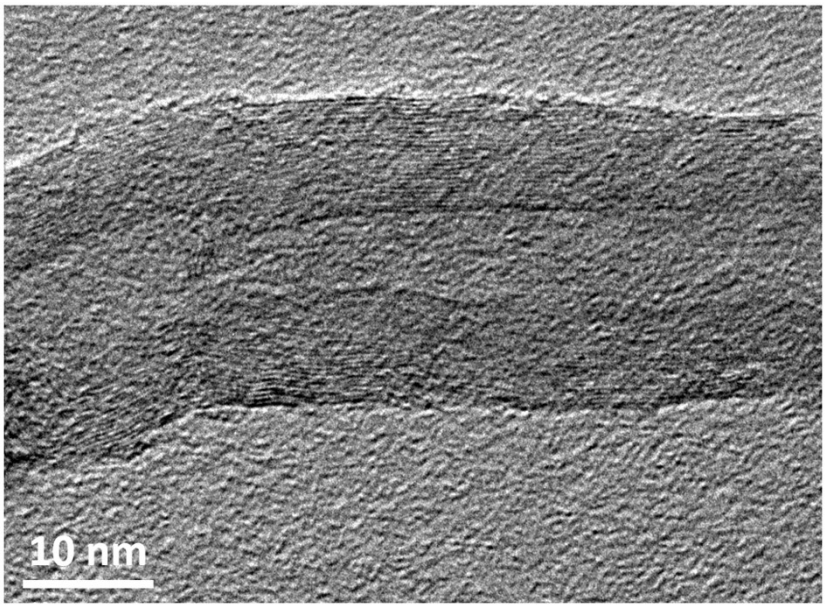

Fig. S3. HRTEM image of CNT.

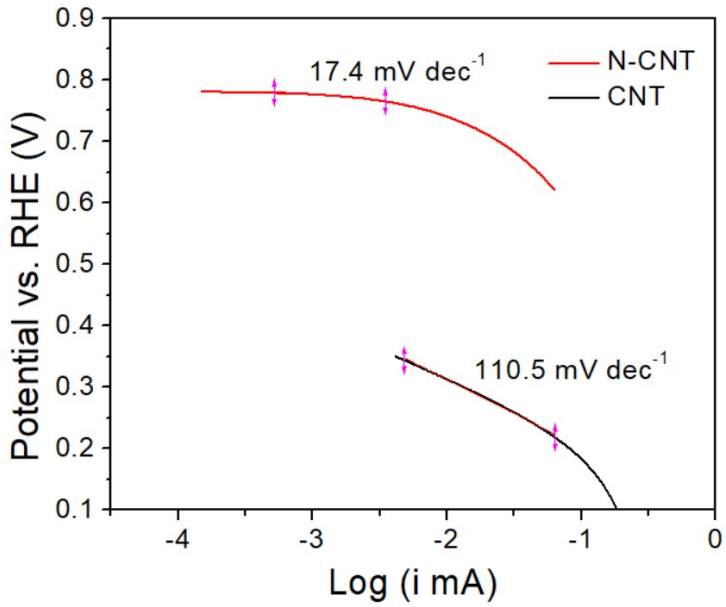

Fig. S4. Tafel plots of CNT and N-CNT for ORR in 0.1 M PBS.

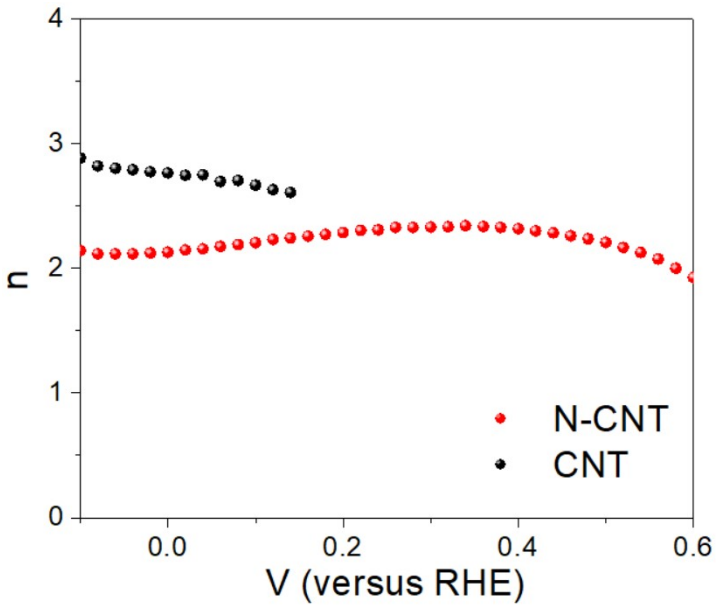

Fig. S5. Calculated electron transfer numbers of CNT and N-CNT in 0.1 M PBS.

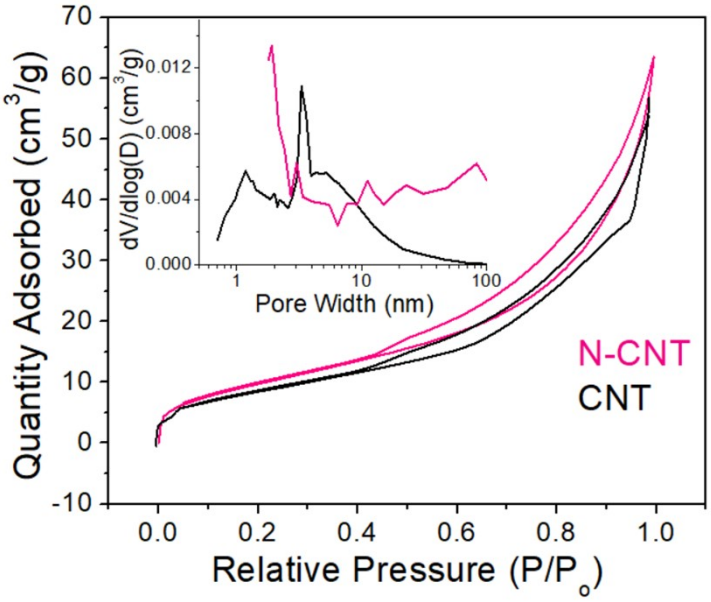

Fig. S6. Nitrogen adsorption–desorption isotherms of CNT and N-CNT. Inset: relevant pore-size distribution.

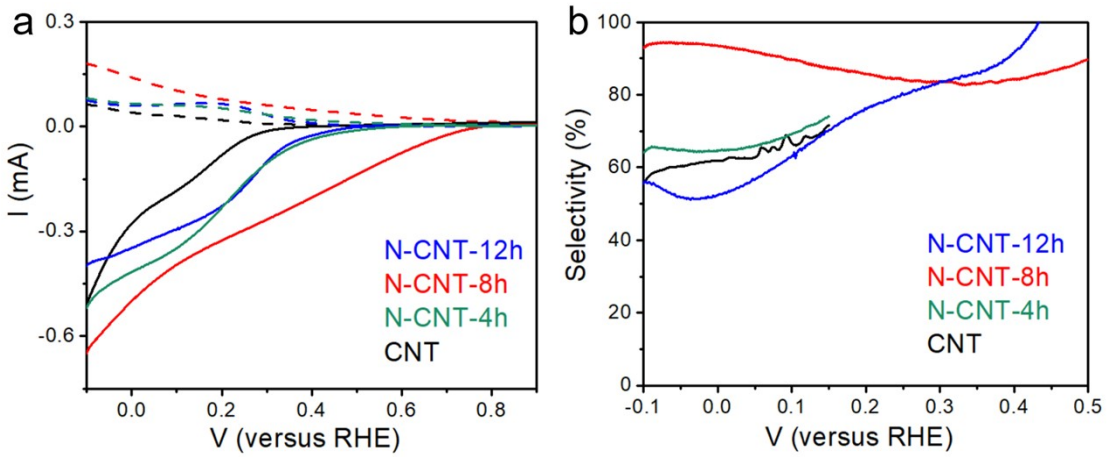

Fig. S7. Influence of reaction time on electrochemical performance. (a) RRDE voltammograms and (b) calculated selectivity of N-CNT for H_2O_2 production in 0.1 M PBS.

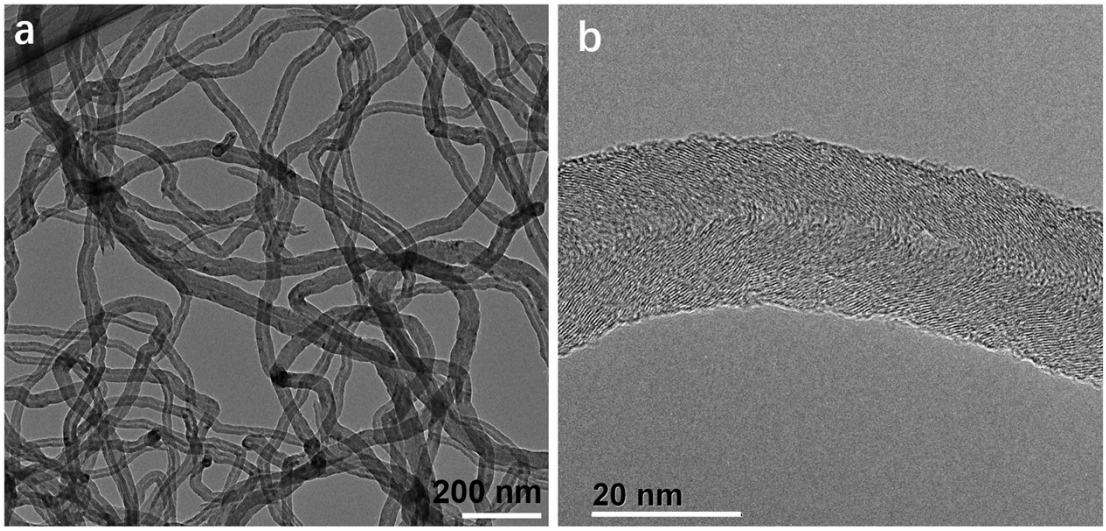

Fig. S8. (a) TEM and (b) HRTEM images for N-CNT after ORR stability test.

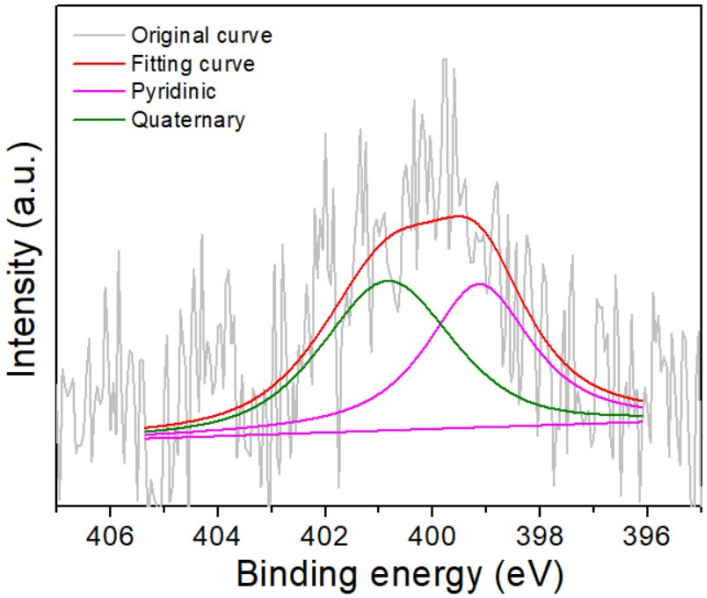

Fig. S9. Deconvoluted N 1s spectra of N-CNT after ORR stability test.

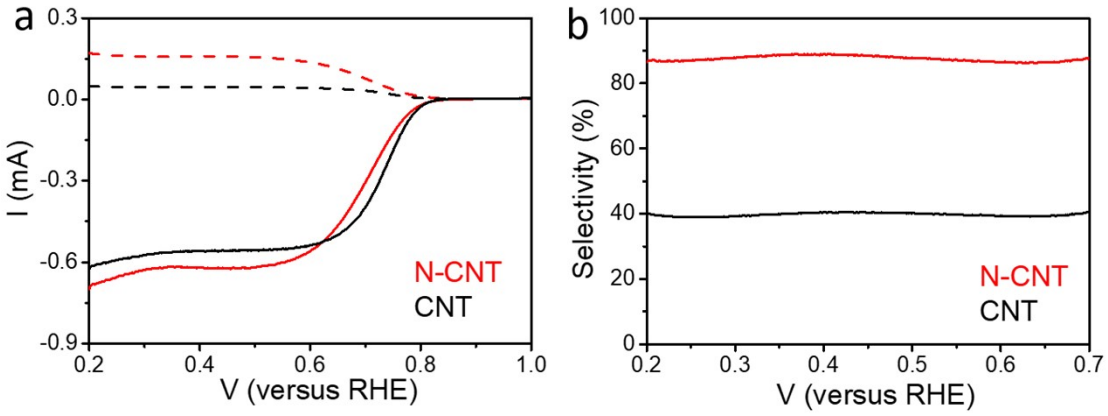

Fig. S10. (a) RRDE voltammograms and (b) Calculated selectivity of CNT and N-CNT for the ORR and H_2O_2 production in 0.1 M KOH.

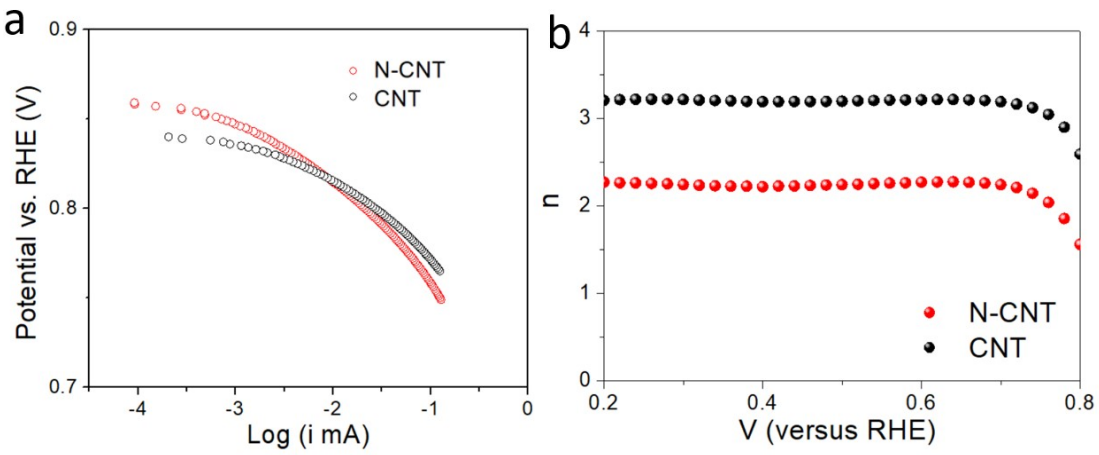

Fig. S11. (a) Tafel plots and (b) Calculated electron transfer numbers of CNT and N-CNT in 0.1 M KOH.

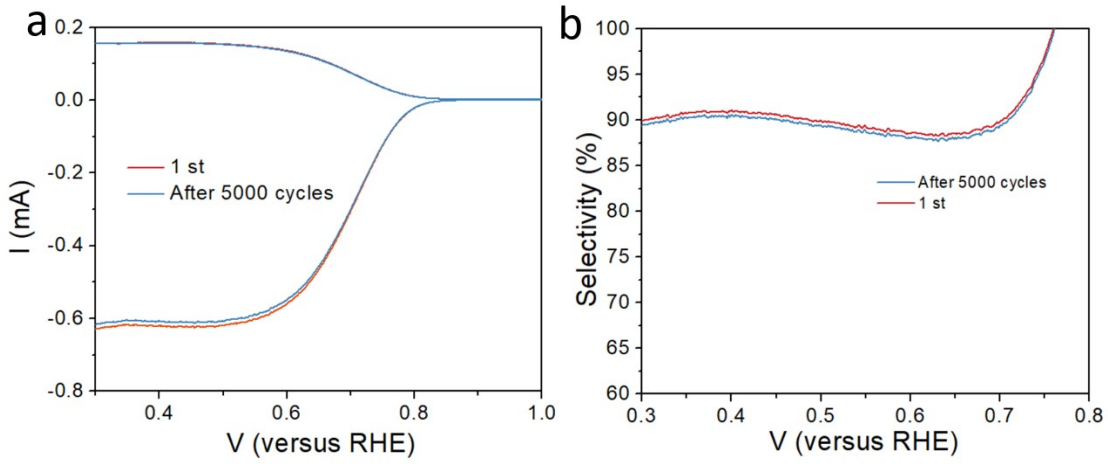

Fig. S12. (a) RRDE voltammograms after 5000 cycles at 1600 rpm in O_2-saturated 0.1 M KOH, and (b) corresponding H_2O_2 selectivity.

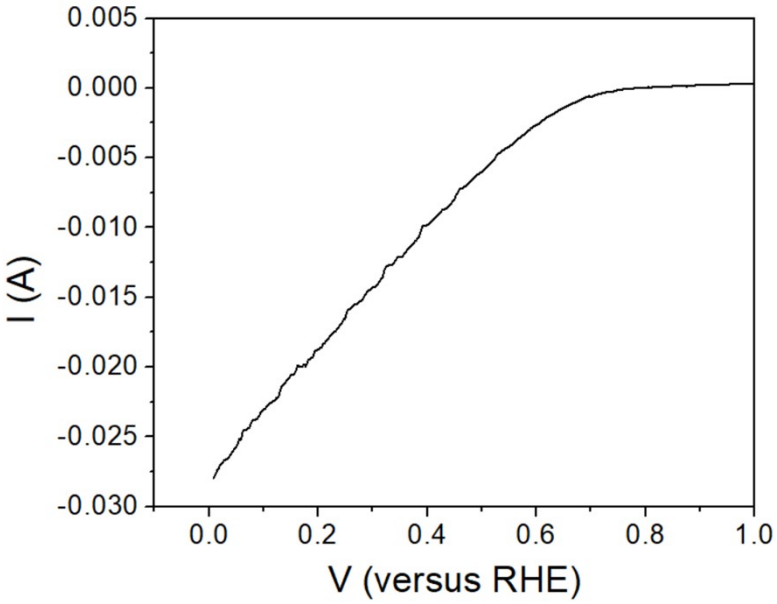

Fig. S13. Polarization curve of N-CNT catalyst for producing H_2O_2 in 0.1 M PBS.

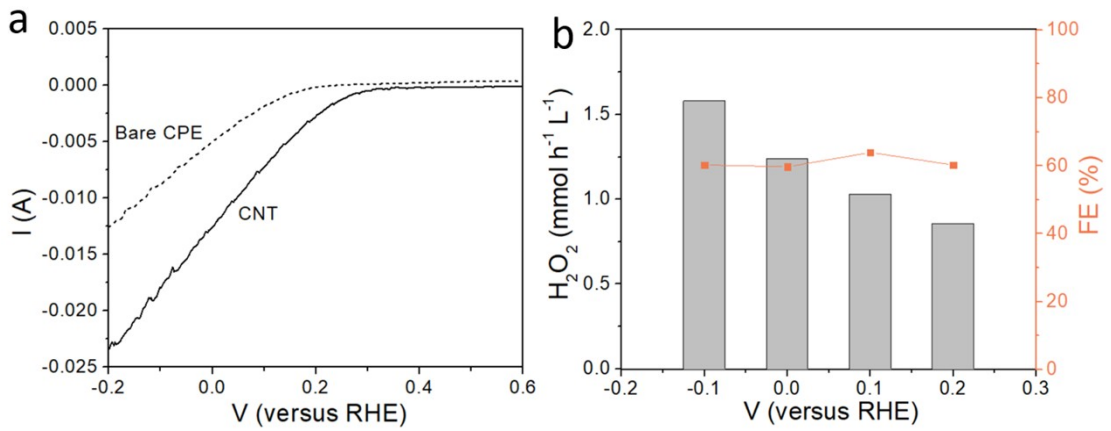

Fig. S14. (a) Polarization curve of Bare CPE and CNT catalyst for producing H_2O_2 in 0.1 M PBS. (b) FEs and H_2O_2 yields over CNT at various potentials in 0.1 M PBS.

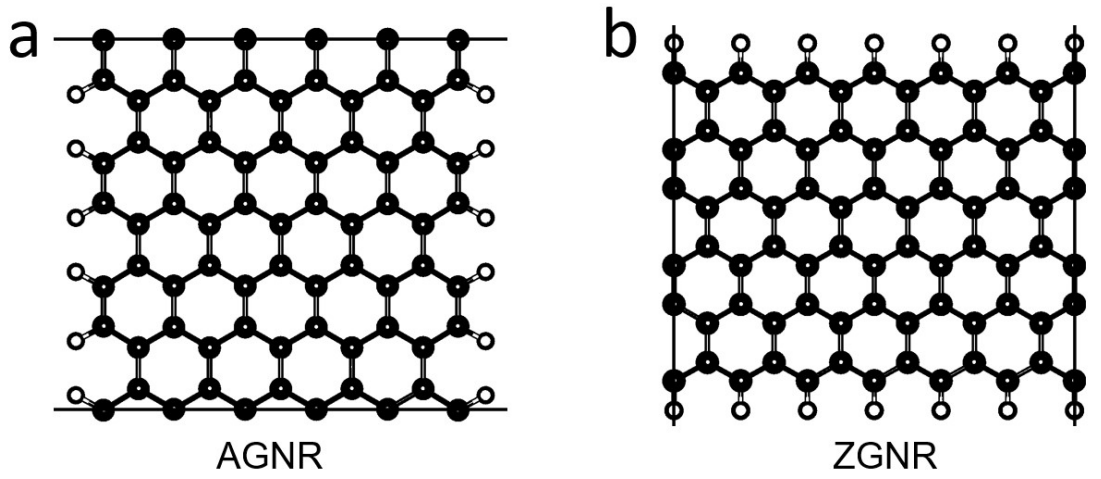

Fig. S15. Atomic structures of the adopted graphene nanoribbon models (AGNR in (a) and ZGNR in (b)), where the black solid lines denote the boundary of the supercell. Dark blue and pink spheres denote C and H atoms, respectively.

Table S1 The influence of elemental content on the H_2O_2 selectivity of N-CNT.

Sample	N by EDX (at. %)	C by EDX (at. %)	O by EDX (at. %)	H_2O_2 selectivity (%) at 0 V vs. RHE
N-CNT-12h	6.08	86.98	6.94	51.6
N-CNT-8h	4.52	88.36	7.12	>90
N-CNT-4h	1.27	88.99	9.74	64.6
CNT	/	96.29	3.71	60.8

Table S2 Comparing the performance of recently reported electrocatalysts for oxygen reduction to H_2O_2.

Electrocatalyst	Electrolyte	Selectivity [%]	Onset potential *vs* RHE	Reference
N-CNT	0.1 M PBS	92.5	0.78	This work
HPC	0.1 M Na_2SO_4	70.8	0.16	12
AC	Deionized water	26.5	0.31	13
Carbon fiber	Ultrapure water	52.0	0.51	14
NCMK3IL50_800T	0.1 M K_2SO_4	75.7	0.2	15
MCHS-9:1	0.1 M PBS	>90	0.57	16
Bi_2Te_3 NPs	0.1 M KOH	100	~0.75	17
Co1-NG(O)	0.1 M KOH	82	0.8	18
	0.1 M $HClO_4$	/	0.7	18
	0.1 M PBS	~60	0.3-0.4	18
N-FLG-8	0.1 M KOH	95	0.8	19
Co-POC-O	0.1 M KOH	84	0.79	20
MOF NSs-300	0.1 M KOH	99	0.75	21
Co-N-C	0.1 M KOH	~60	~0.82	22
	0.5 M H_2SO_4	~80	~0.78	22
Mo1/OSG-H	0.1 M KOH	95	0.8	23
O-CNTs	0.1 M KOH	90	0.8	24
	0.1 M PBS			
F-mrGO(600)	0.1 M KOH	100%	0.7	25
BN-C1	0.1 M KOH	90%	0.8	26

Table S3 H_2O_2 productivity comparison.

Electrocatalyst	Electrolyte	Productivity	Reference
N-CNT	0.1 M PBS	~4.45 mmol $L^{-1}h^{-1}$	This work
HPC	0.1 M Na_2SO_4	110.2 mmol h^{-1} g^{-1}	12
AC	Deionized water	74.2 μmol h^{-1}	13
Carbon fiber	Ultrapure water	57 μg h^{-1} mg^{-1}	14
NCMK3IL50_800T	0.1 M K_2SO_4	561.7 mmol $g_{catal.}^{-1}$ h^{-1}	15
MCHS-9:1	0.1 M PBS	/	16
Bi_2Te_3 NPs	0.1 M KOH	6.36 mmol L^{-1} h^{-1}	17
Co1-NG(O)	0.1 M KOH	~418 mmol g^{-1} h^{-1}	18
N-FLG-8	0.1 M KOH	~9.66 mol $g_{cat}^{-1}h^{-1}$	19
Co–POC–O	0.1 M KOH	813 mg L^{-1} h^{-1}	20
MOF NSs-300	0.1 M KOH	~6.5 mol $g_{cat}^{-1}h^{-1}$	21
Co−N−C	0.1 M KOH	~4.33 mol $g_{cat}^{-1}h^{-1}$	22

References

1 G. Kresse, J. Furthmüller, *Phys. Rev. B* 1996, **54**, 11169.

2 P. E. Blöchl, *Phys. Rev. B* 1994, **50**, 17953−17979.

3 J. P. Perdew, K. Burke, M. Ernzerhof, *Rev. Lett.* 1996, **77**, 3865−3868.

4 S. Grimme, J. Antony, S. Ehrlich, H. Krieg, *J. Chem. Phys.* 2010, **132**, 154104.

5 H. J. Monkhorst, J. D. Pack, *Phys. Rev. B* 1976, **13**, 5188−5192.

6 S. Siahrostami, A. Verdaguer-Casadevall, M. Karamad, D. Deiana, P. Malacrida, B. Wickman, M. Escudero-Escribano, E. A. Paoli, R. Frydendal, T. W. I. Hansen, Chorkendorff, I. E. L. Stephens, J. Rossmeisl, *Nat. Mater.* 2013, **12**, 1137−1143.

7 Z. Lu, G. Chen, S. Siahrostami, Z. Chen, K. Liu, J. Xie, L. Liao, T. Wu, D. Lin, Y. Liu, T. F. Jaramillo, J. K. Nørskov, Y. Cui, *Nat. Catal.* 2018, **1**, 156–162.

8 X. Zhao, Y. Wang, Y. Da, X. Wang, T. Wang, M. Xu, X. He, W. Zhou, Y. Li, J. N. Coleman, Y. Li, *Natl. Sci. Rev.* 2020, **7**, 1360–1366.

9 G. F. Han, F. Li, W. Zou, M. Karamad, J. P. Jeon, S. W. Kim, S. J. Kim, Y. Bu, Z. Fu, Y. Lu, S. Siahrostami, J. B. Baek, *Nat. Commun.* 2020, **11**, 2209.

10 J. K. Nørskov, J. Rossmeisl, A. Logadottir, L. Lindqvist, J. R. Kitchin, T. Bligaard, H. Jónsson, *J. Phys. Chem. B* 2004, **108**, 17886−17892.

11 http://webbook.nist.gov/chemistry/.

12 Y. Liu, X. Quan, X. Fan, H. Wang and S. Chen, *Angew. Chem. Int. Ed.* 2015, **54**, 6837–6841.

13 I. Yamanaka and T. Murayama, *Angew. Chem. Int. Ed*. 2008, **120**, 1926–1928.

14 J. Choi, S. H. Hwang, J. Jang and J. Yoon, *Electrochem. commun.*, 2013, **30**, 95–98.

15 Y. Sun, I. Sinev, W. Ju, A. Bergmann, S. Dresp, S. Kühl, C. Spöri, H. Schmies, H. Wang, D. Bernsmeier, B. Paul, R. Schmack, R. Kraehnert, B. Roldan Cuenya and P. Strasser, *ACS Catal.*, 2018, **8**, 2844–2856.

16 Y. Pang, K. Wang, H. Xie, Y. Sun, M. M. Titirici and G. L. Chai, *ACS Catal.*,

2020, **10**, 7434–7442.

17 N. Zhang, F. Zheng, B. Huang, Y. Ji, Q. Shao, Y. Li, X. Xiao, X. Huang, *Adv. Mater.* 2020, **32**, 1906477.

18 E. Jung, H. Shin, B. H. Lee, V. Efremov, S. Lee, H. S. Lee, J. Kim, W. Hooch Antink, S. Park, K. S. Lee, S. P. Cho, J. S. Yoo, Y. E. Sung, T. Hyeon, *Nat. Mater*. 2020, **19**, 436-442.

19 L. Li, C. Tang, Y. Zheng, B. Xia, X. Zhou, H. Xu, S. Z. Qiao, *Adv. Energy Mater*. 2020, **10**, 2000789.

20 B. Li, C. Zhao, J. Liu, Q. Zhang, *Adv. Mater*. 2019, **31**, 1808173.

21 M. Wang, N. Zhang, Y. Feng, Z. Hu, Q. Shao, X. Huang, *Angew. Chem. Int. Ed*. 2020, **59**, 14373-14377.

22 Y. Sun, A. Bagger, N. Ranjbar, W. Ju, J. Li, A. Zitolo, S. Li, L. Silvioli, L. Arnarson, X. Wang, T. Möller, D. Bernsmeier, J. Rossmeisl, F. Jaouen, P. Strasser, *J. Am. Chem. Soc*. 2019, **141**, 12372-12381.

23 C. Tang, Y. Jiao, B. Shi, J. Liu, Z. Xie, X. Chen, Q. Zhang, S. Qiao, *Angew. Chem. Int. Ed*. 2020, **132**, 9256-9261.

24 Z. Lu, G. Chen, S. Siahrostami, Z. Chen, K. Liu, J. Xie, L. Liao, T. Wu, D. Lin, Y. Liu, T. F. Jaramillo, J. K. Nørskov, Y. Cui, *Nat. Catal*. 2018, **1**, 156–162.

25 H. W. Kim, M. B. Ross, N. Kornienko, L. Zhang, J. Guo, P. Yang, B. D. McCloskey, *Nat. Catal*. 2018, **1**, 282-290.

26 S. Chen, Z. Chen, S. Siahrostami, D. Higgins, D. Nordlund, D. Sokaras, T. R. Kim, Y. Liu, X. Yan, E. Nilsson, R. Sinclair, J. K. Nørskov, T. F. Jaramillo, Z. Bao, *J. Am. Chem. Soc*. 2018, **140**, 7851-7859.